Novel high-efficiency plasma nitriding process utilizing a high power impulse magnetron sputtering discharge

EHIASARIAN, A.P. <http://orcid.org/0000-0001-6080-3946> and HOVSEPIAN, P. Eh <http://orcid.org/0000-0002-1047-0407>

Journal of Vacuum Science and Technology A

RESEARCH ARTICLE | FEBRUARY 28 2024

Novel high-efficiency plasma nitriding process utilizing a high power impulse magnetron sputtering discharge

Special Collection: Celebrating the Achievements and Life of Joe Greene

A. P. Ehiasarian ; P. Eh. Hovsepian

J. Vac. Sci. Technol. A 42, 023109 (2024)
https://doi.org/10.1116/6.0003277

JVST A
Journal of Vacuum Science & Technology A

ARTICLE

pubs.aip.org/avs/jva

Novel high-efficiency plasma nitriding process utilizing a high power impulse magnetron sputtering discharge

Cite as: J. Vac. Sci. Technol. A **42**, 023109 (2024); doi: 10.1116/6.0003277
Submitted: 3 November 2023 · Accepted: 25 January 2024 ·
Published Online: 28 February 2024

A. P. Ehiasarian[a] and P. Eh. Hovsepian

AFFILIATIONS

National HIPIMS Technology Centre, Sheffield Hallam University, Howard St, Sheffield S1 1WB, United Kingdom

Note: This paper is part of the Special Topic Collection Celebrating the Achievements and Life of Joe Greene.
[a]**Electronic mail:** a.ehiasarian@shu.ac.uk

ABSTRACT

Lifetime and biocompatibility of orthopedic implants are crucial in meeting the new challenges brought about by the fall in the patient age and the aging population. The high-load surfaces in contact with the biological environment must display enhanced tribological properties, biocompatibility, and reduced metal ion release in long-term clinical performance. Surface modification techniques such as nitriding can significantly improve the in-service behavior of the medical-grade alloys in current use. We report on a novel approach for nitriding of CoCrMo alloys using high power impulse magnetron sputtering (HIPIMS) discharge. The new nitriding process has been successfully carried out at the National HIPIMS Technology Centre at Sheffield Hallam University, UK, in an industrial size Hauzer 1000-4 system enabled with HIPIMS technology. While the nitriding ion flux is controlled by the HIPIMS magnetron plasma source, the ion energy can be independently set via the substrate bias. Implementing the HIPIMS source allows reducing the operational pressure by one order of magnitude compared to conventional dc plasma nitriding (DCPN). Plasma analyses have identified significantly enhanced production of ions of molecular nitrogen (N_2^+), atomic nitrogen (N^+), and N_2H^+ radicals in the HIPIMS discharge compared to DCPN. Because of the low pressure of operation of the HIPIMS process, the energy of ions is similar to the bias voltage, whereas the high pressures used in DCPN cause severe losses in ion energy due to scattering collisions within the sheath. The high flux and high ion energy are primarily responsible for achieving a fourfold increase in process productivity as compared to state-of-the-art plasma nitriding processes. The nitrided surface layers exhibit excellent mechanical and tribological properties, which bring about significant improvements in hardness, fracture toughness, and wear. The protective function of the nitrided layer against corrosion in the aggressive environments of simulated body fluid is remarkably augmented. The barrier properties of the nitrided layer have been demonstrated through a reduction in metal ion release by as much as a factor of 2, 4, and 10 for Co, Cr, and Mo, respectively.

I. INTRODUCTION

Surface modification by chemical heat treatments is universally used to extend the functionality of engineering components to help them enhance their wear resistance and anticorrosion characteristics in aggressive media. Significant performance gains can be made through combination with coating technologies such as physical vapor deposition, which typically produce a layer of ceramic material tailored to withstand the operational conditions of the component. However, conventional treatments are slow and energy intensive as they rely on the heat-activated diffusion of active species into the solid component. Moreover, the processes of treatment and coating are traditionally carried out in separate vacuum reactors, requiring time and energy for cooling down, reheating, and decontamination after transfer, thereby introducing inefficiencies in the use of energy and duration of the production process. Duplex treatments, whereby both processes are carried out in the same equipment, are a promising alternative. However, there are persistent challenges first in developing large-area plasma sources with sufficient density to accelerate the chemical heat treatment

process and second, in achieving compatibility between the treatment and PVD coating processes.

Chemical heat treatment is conducted at high temperatures in a solid, liquid, or gaseous environment that contains reactive species that enrich the surface of the material up to a certain case depth and thereby modify its properties. Nitriding is one of the most widely spread chemical heat treatment processes where the surface is enriched by nitrogen. Metallurgist Adolph Machlet developed nitriding by accident in 1906 in an experiment where he replaced the air atmosphere in a furnace with ammonia to avoid oxidation of steel parts.

In the gaseous environment, the duration of the process is determined by the rate of three elementary processes. The first process is dissociation, where the gas molecules are decomposed to gas atoms followed by surface absorption of these active species and their inward diffusion. The kinetics of these three processes is determined by the applied temperature, therefore, process intensification is highly limited.

A significant breakthrough in process intensification was achieved when the reactivity of the gaseous process environment was enhanced by ionizing it. Direct current plasma nitriding (DCPN) also referred to as ion-nitriding was invented by Wehnheldt and Berghaus in 1932 where the DC glow discharge phenomenon is used to introduce nascent nitrogen to the surface.[1] In plasma nitriding, the reactivity of the nitriding media is not driven by heat but by the ionized state of the gas. In its original version, the process is carried out under high pressure (100–1000 Pa) in a high-voltage (0.3–1 kV) DC glow discharge sustained between the treated component acting as a cathode and the chamber walls acting as an anode. The bulk plasma created by the discharge is absorbed by contacting surfaces. The light, highly mobile electrons are absorbed over longer distances from the surface than the heavy, almost stationary ions. This imbalance leads to the formation of a zone of positive charge called the plasma sheath around each surface in contact with the plasma. In the sheath, the ion and electron density are both reducing exponentially toward the surface, however, the reduction in ion density is negligible, whereas the electron population is practically eliminated. The sheath width adjusts itself to establish an equilibrium between the fluxes of ions and electrons to the surface. With the flux defined as the product of the density and velocity of the particles, the flux of the slow ions can be balanced with an electron density, which is a fraction of that of the ions. The sheath width expands with applied voltage and contracts with plasma density. Ions in the bulk plasma are accelerated toward the sheath by small electric fields sustained by small local differences in charge density and enter it at the Bohm velocity, which is equivalent to the energy of a few electron volts. They then experience substantial acceleration to a few hundred electron volts by the electric field established between the potential of the surface (applied voltage) and the potential of the bulk plasma (a few volts above ground).

The abnormal form of the discharge has been applied to access higher density plasma and achieve full coverage of the treated surface;[2] however, case depth variations are often observed for components with complex 3D shapes. This is caused by the focusing of the electric field toward the tips of sharp features on the parts, which reduces the local plasma sheath width and attracts more ion flux relative to the flat surfaces.

With the introduction of the pulsed discharge, this drawback was largely eliminated, and the nitriding rate significantly increased.[3,4] Here, the voltage is pulsed to several hundred volts, bringing about a rapid expansion of the plasma sheath. A fast voltage rise is crucial to ensure that the light electrons can respond to the change in the electric field and leave the vicinity of the substrate, while heavier ions remain stationary forming a matrix sheath. In this case, the ions retain their density and are exposed to the field in the expanded sheath, which eventually accelerates them perpendicular to the surface.

One clear feature of DCPN, however, is the strong coupling of the substrate temperature and the plasma reactivity in the gaseous phase with the discharge parameters. Decoupling of the substrate temperature and the plasma reactivity and substantial decrease of the process pressure to the range of 0.4–10 Pa have been achieved by the utilization of the high frequency (13.56 MHz) rf discharge, triode arrangement,[5,6] and use of the electron cyclotron resonance (ECR) microwave plasma.[7]

In the mid-1970s, nitrogen ion implantation technology was developed.[8] To be carried out, the process requires the use of an ion implanter usually utilizing a Kaufman ion source,[9] which can deliver ions with energies as high as 50–150 keV and surface interaction doses in the range of 10^{17} ions cm^{-2}. The maximum penetration of the ions, which defines the hardened case depth, is a function of the atomic numbers and masses of the incident species and substrate elements and the energy and angle of incidence of the ion beam. One of the disadvantages of the ion implantation technology is that it is a line-of-sight process, which requires the use of manipulators to adequately expose the treated surfaces to the beam.

A more advanced version of the ion implantation technology called plasma source ion implantation (PSII) was developed in 1987 by Conrad and co-workers in Wisconsin, USA.[10] In PSII, the component is placed directly in the plasma source and is pulse-biased to very high negative potentials of −10 to −100 kV relative to the chamber walls. In response, the plasma sheath around the substrate expands significantly reaching several 10 s of centimeters, thus achieving a near-uniform coverage over typical features such as cutting edges. This largely overcomes the line-of-sight restriction[10] associated with abnormal glow discharges.

Various plasma sources have been used to execute the technology. One advantageous variation of this process is when the plasma is generated and maintained by electron-neutral gas collisions, where the electrons are produced by thermo-electron emission from a hot filament and drawn to the anode (vacuum chamber walls). A particularly effective plasma nitriding process was obtained by the thermionic arc evaporation process,[11,12] where a high-current (100–300 A), low-voltage (25–40 V) thermionic arc is generated in Ar atmosphere in an ionization chamber, whereas segmented anodes located in the process chamber distribute the plasma uniformly for nitriding. With the application of a low voltage on the parts that are immersed in the plasma, ions are drawn and implanted into the surface of the parts.[13,14]

A system like this can be combined with a coating process to achieve duplex treatment.[15] The duplex treatment comprises a preliminary nitriding treatment followed by the deposition of a hard coating. By combining these two processes, a composite layer is

formed where the thin ceramic coating is efficiently supported by the enhanced load-bearing capacity of the nitrided substrate surface. The nitrided layer has an intermediate graded modulus of elasticity, which enables a smoother transition between the high elastic modulus of the coating and the low one of the substrate, and leads to superior fatigue and wear resistance of the system.

The duplex treatment reveals most fully the advantages of the nitriding process. However, not all the above variations of nitriding are suitable for combination with coating and can deliver an economically viable technology. In some cases, a duplex treatment can be achieved only by using two separate process systems: a nitriding unit and a coating deposition system, which is a slow and costly approach. In cases where the two stages of the technology are combined in a single unit, separate sources are used for nitriding and for coating deposition, which renders the approach economically challenging.

The current paper reports on an alternative solution for duplex treatment in a single unit where nitriding and the coating deposition are carried out for the first time by using a single source: a magnetron device driven in the high power impulse magnetron sputtering (HIPIMS) mode.

HIPIMS is an innovative magnetron sputtering technique, which employs short pulses with high power density to produce highly ionized plasma.[16] It was upscaled for the first time in 2003 at Sheffield Hallam University, UK, by Professors A. P. Ehiasarian and P. Eh. Hovsepian.[17] Conventionally used to augment coating deposition, the HIPIMS discharge has been found to be well suited to enhancing plasma nitriding at low pressure in the range of 10^{-1} Pa due to its efficient production of molecular (N_2^+) and atomic nitrogen (N^+) ion species, which are the primary catalysts for the formation of nitrided layers.[18] The current study is dedicated to the comprehensive evaluation of the HIPIMS-enhanced low-pressure plasma nitriding (HLPPN) technology in terms of plasma characteristics, nitriding case depth, phase composition of the nitrided layer, fracture toughness, wear resistance, and corrosion properties. All these features are presented for the case of CoCrMo (F75) alloys and in relation to conventional DCPN and the untreated substrate.

II. EXPERIMENTAL DETAILS

A. HIPIMS enhanced low-pressure plasma nitriding technique

The novel plasma nitriding was carried out in an industrial size (chamber volume of 1 m^3) HTC 1000–4, four-cathode system (Hauzer Techno Coatings, Europe B.V., Venlo, The Netherlands) enabled with HIPIMS technology at the UK National Centre for HIPIMS Technology at Sheffield Hallam University. The system is equipped with two HIPIMS power supplies (Hüttinger Elektronik Sp. z o.o., Warsaw, Poland). The cathodes were furnished with two Cr and two Nb targets of 99.99% purity. The samples have been mounted on a centrally placed rotating substrate table capable of threefold planetary rotation, which helps achieve uniform coverage or plasma exposure of complex 3D-shaped components. The substrates can be suitably biased with the help of a dedicated bias power supply capable of handling elevated currents associated with highly ionized depositing flux (Hüttinger Elektronik Sp. z o.o., Warsaw, Poland).[19] The four rectangular cathodes can be operated in either direct current unbalanced magnetron sputtering (UBM) or HIPIMS mode. Figure 1 shows a schematic cross-sectional view of the machine depicting the four-cathode arrangement.

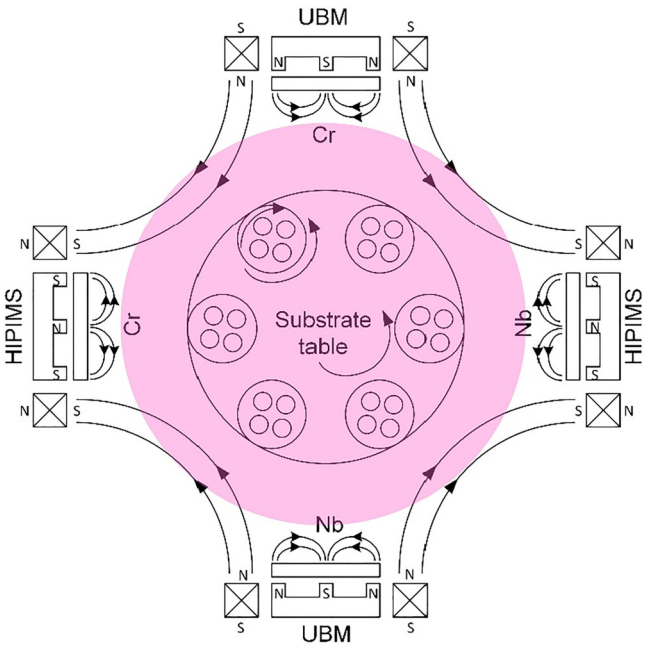

FIG. 1. Schematic cross-sectional view of the HTC 1000-4 machine enabled with HIPIMS technology depicting the four-cathode arrangement.

Prior to plasma nitriding, the substrate surface was pretreated by a HIPIMS plasma discharge maintained on one Cr target in pure Ar atmosphere. During this step, a high bias voltage typically Ub = − 1000 V is applied to the samples. In these conditions, the substrate surface is subjected to intensive bombardment by Cr^+ ions, which remove organic contaminants and oxide layers by sputtering, but more importantly, the process results in shallow metal ion implantation with a range of up to 10–15 nm into the irradiated substrate material.[20]

In the next step, for this particular study, the nitriding process was carried out for 4 h in a mixed (N_2 + 15%H_2) atmosphere. Plasma was produced by maintaining HIPIMS discharge on one pair of Cr and Nb targets and a UBM discharge on a second pair of Cr and Nb targets. The target materials can be selected and varied according to the constitution of the subsequently deposited functional coating if a duplex process is executed. Similarly, the number of the HIPIMS cathodes involved in the coating deposition step can be selected based on considerations discussed elsewhere.[21] To avoid coating deposition on the ion bombarded surface of the samples during HLPPN, the power on the magnetrons was kept very low, whereas the applied bias voltage was selected high in order to guarantee intensive substrate surface sputtering. The substrate bias voltage during nitriding was kept in the range of −900 to −1000 V where the system was operated in a voltage-controlled

(VC) mode. Time-resolved measurements of the substrate bias voltage using an oscilloscope confirmed that deviations were within 1% of the set voltage throughout the HIPIMS power pulse on the magnetrons. No significant change in substrate current was observed for different voltages confirming that the plasma is primarily generated at the magnetron cathodes and the contribution of any auxiliary discharge on the substrate surface can be neglected. The substrate temperature was measured through an isolation transformer using a thermocouple encapsulated in a steel sheath and placed inside a steel dummy substrate, which was mounted on the substrate carousel and rotated and biased in an identical way to the nitrided parts. The substrate temperature and the total pressure were kept constant at 400 °C and 8×10^{-3} mbar, respectively. The system was operated in a pressure control mode using an SRG-3 Spinning Rotor Vacuum Gauge System (MKS Instruments) and gas flow controllers.

Nitriding was carried out on metallurgically polished (1 μm diamond paste finish) CoCrMo alloy disks with Ø = 26 mm and a thickness of 5 mm.

For benchmarking purposes, a similar set of samples was also nitrided using state-of-the-art commercially available equipment and following an industrially accepted and approved technological process based on pulsed DC glow discharge plasma nitriding (DCPN). In these trials, the nitriding was carried out in a mixed ($N_2 + H_2$) atmosphere at constant pressure in the range of 10^{-2} mbar. The process temperature was held at around 400 °C for a duration of 18 h.

B. Plasma diagnostic techniques

To compare the plasma characteristics in HLPPN and DCPN processes, a separate chamber equipped with a host of plasma diagnostic systems was used to replicate the respective process conditions and diagnose the plasma flux arriving at the substrate. Figure 2 is a schematic of the cylindrical UHV system showing the position of the substrate, magnetron, energy-resolved mass spectrometer, and Langmuir probe used for the analyses. The base pressure was $<3 \times 10^{-7}$ mbar. An unbalanced planar magnetron (Torus™, Kurt J Lesker) with a diameter of 75 mm was furnished with a Cr target. The stronger outer magnets of the unbalanced configuration project the magnetic field normal to the target surface, thereby significantly enhancing the plasma flux to the substrate.

The substrate was positioned 15 cm from the target surface. The substrate (diameter 75 mm) was placed in a conducting ring holder with a diameter of 110 mm; the substrate recess was 1 mm. The substrate and holder assembly had an area of 95 cm^2 and was used as the main cathode during conventional nitriding. A grounded shield with dimensions 170×200 mm was placed concentrically in the plane with the substrate holder and insulated from it with a gap of 3 mm. The substrates were biased using a high-voltage DC power supply type LH (Glassman High Voltage Inc.) equipped with a smoothing capacitor bank to enable the voltage to be maintained during high current transients on the substrate. Bias voltages of up to −1600 V were used.

The discharge was operated in a fully reactive $N_2 + 15\%H_2$ atmosphere administered from a premixed gas cylinder. The gas

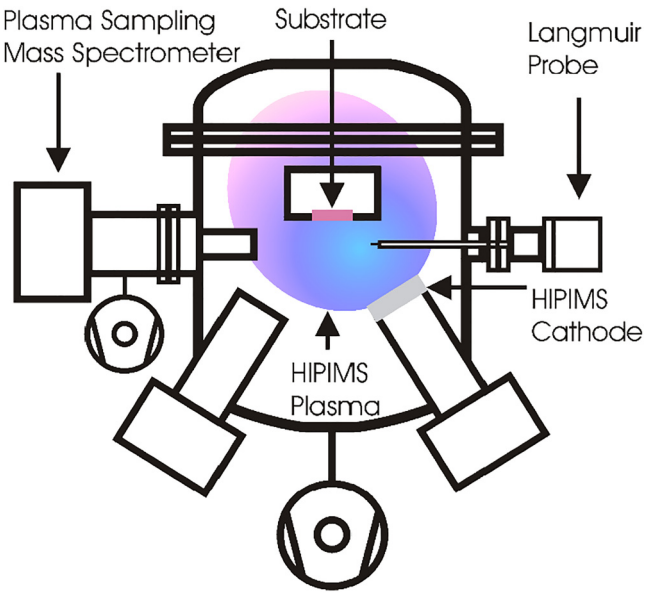

FIG. 2. Schematic of the vacuum system with various plasma diagnostics devices.

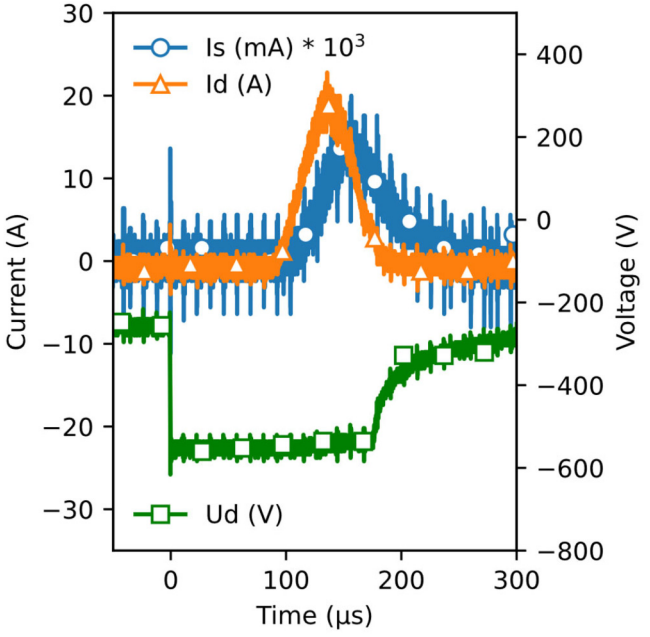

FIG. 3. Cathode voltage, cathode current, and substrate current waveforms during HIPIMS-enhanced low pressure plasma nitriding, illustrating the role of the cathode as a primary plasma source contributing to the majority of substrate current.

pressure was measured using a viscosity pressure gauge (SRG-2 from MKS Instruments). A throttle valve was used to set the pumping speed and enable the turbomolecular pumps to operate at high pressures.

The working pressure during HLPPN was 8.300×10^{-3} mbar at a gas flow of 83 SCCM. During DCPN, the pressure was 9.255×10^{-2} mbar at a gas flow of 100 SCCM. The pressure during DCPN was identical to the pressure used in commercial plasma nitriding plants.

To perform HLPPN, the magnetron was driven with a HIPIMS power supply (HMP 2/1 from Hüttinger Electronic Sp. z O.O.) at a pulse frequency of 208 Hz, pulse duration of 100 μs, and duty cycle of 2%. The peak discharge current I_d was 22 A (peak current density of 0.480 A cm^{-2}), and the average discharge current was 1.27 A (26 mA cm^{-2}) at a peak voltage of −500 V. The discharge current and voltage were monitored at the output of the power supply with a Pearson™ current monitor (model 110) with attenuation of 10 mA/mV and a high voltage probe type P5100 (Tektronix®) with attenuation of 100×, respectively. The substrate current was measured using a current clamp probe type P6021A (Tektronix®) set to an attenuation of 2 mA/mV. The waveforms were recorded using a digital oscilloscope (DPO7054 from Tektronix®). Figure 3 in Sec. III A shows the current and voltage waveforms.

To perform DCPN, the substrate was biased, and the magnetron was switched off. The substrate current was measured using a digital current meter (MX547 from ITT Instruments Metrix).

1. Energy-resolved mass spectroscopy with biased sampling orifice

The energy and composition of ions in the nitriding flux were measured using a differentially pumped energy-resolved mass spectrometer model PSM003 (Hiden Analytical Ltd.). The distance from the plasma-sampling orifice of the analyzer to the magnetron was 170 mm. Measurements were taken in the time-averaged mode. To enable an accurate determination of the flux to the substrates during DCPN, the plate carrying the sampling orifice of the spectrometer was used as a cathode in the system. A DCPN discharge was ignited on the sampling orifice plate by biasing it to −400 V using a high-voltage DC power supply model LH (Glassman High Voltage Inc.). Using this arrangement, both DCPN and HLPPN nitriding conditions were replicated and ion energy distribution functions were obtained at the working pressures cited above. During HLPPN, the main discharge was obtained from the magnetron and the biased spectrometer orifice plate assumed the role of the biased substrate. The spectrometer was tuned so that the lens and extractor voltages were 100 V higher than the voltage applied to the orifice in order to enable full deceleration of the ions within the instrument and detection of energies down to 0 eV. In terms of composition, we appreciate that the spectrometer measures particle flux ratios; however, we assume they represent density ratios as the energies of ions were similar.

2. Langmuir probe measurements

Plasma density and electron temperature were characterized by a Langmuir probe system type ESP*ION* (Hiden Analytical Ltd.). Data collection was synchronized with the peak current of the discharge by feeding the current monitor signal into a delay generator type DG535 (Stanford Research Systems), which provided a transistor–transistor logic (TTL) trigger signal to the ESP*ION*.

The Langmuir probe was cylindrical (diameter 150 μm × 10 mm) made of tungsten wire. The ratio of the probe radius (r_p) to the Debye length reached its minimum value of 4.1 at the peak of the pulse. The signal-to-noise ratio in the I–V characteristic was reduced by averaging over 3 scans. The minimum time to collect a single probe I–V characteristic was 30 ms. The voltage step was set to 0.025 V. The cleanliness of the probe surface was maintained by applying a short negative voltage of −150 V between measurements to sputter off any contamination. The probe was positioned at a distance of 12 cm from the target. The local magnetic field flux was 0.45 mT producing a Larmour electron precession radius of $r_L \sim 6.8$ mm for a typical energy of $T_e \sim 2$ eV. Since $r_L > r_p$, the influence of the magnetic field on electron probe collection was neglected. The plasma potential V_p was determined from the knee of the I–V curve at the transition to the electron saturation current region.

C. Material analysis techniques used to characterize the nitrided layer

1. Phase composition

The phase composition of the nitrided and untreated CoCrMo alloy was obtained from an Empyrean x-ray diffractometer with Cu $K\alpha$ radiation (1.5418 Å). The texture coefficient (T*) of the nitrided CoCrMo alloy was investigated using glancing angle incidence mode (2°) and θ–2θ geometry.

The texture coefficient was calculated using the following equation:[22]

$$T^{*} = \frac{I_{hkl}/R_{hkl}}{(1/n)\sum_{0}^{n}(I_{hkl}/R_{hkl})}, \quad (1)$$

where I_{hkl} is the measured peak intensity from the (hkl) reflections, R_{hkl} is the reference standard (random) peak intensity from the (hkl) reflections, and n is the number of reflections considered.

2. Nanohardness

A CSEM-Anton Paar nanohardness tester equipped with a Berkovich diamond tip was used to measure the instrumental hardness (H_{IT}) and elastic modulus (E) of the nitrided and untreated specimens. A fixed load of 20 mN was used to indent the specimens resulting in an indentation depth of less than 10% of the nitrided layer thickness.[23] The nanoindentation hardness value was calculated as an average of 20 indentations.

3. Friction and wear testing

The friction behavior of nitrided layers produced by the different techniques was studied with a CSEM room temperature pin-on-disc tribometer. The counterpart was a 6 mm diameter Al_2O_3 ball under a static load of 5 N. The coefficient of friction $\mu = F_T/F_N$ was calculated during the experiment using a measured value for the tangential force F_T and a fixed normal force F_N

exerted by a calibrated weight. The wear coefficient was calculated using Archard's equation as

$$K_C = \frac{V}{F_N \times d}, \tag{2}$$

where V is the wear volume in m^3, F_N is the normal load in N, and d is the sliding distance in meters. The volume of the wear track (V) on the coated disk is calculated using the equation $V = 2\pi RA$, where R is the wear track radius and A is the cross-sectional area of the wear track. The area of the wear track was calculated from surface profiles obtained by a DEKTAK 150 instrument using its associated software. The profile scanning was repeated for 8–10 times on different sections of the wear track and the average was considered as area A, which was used in Eq. (2). The wear coefficients of the counterparts were calculated from the worn area measured with the help of an optical microscope.

4. Fracture toughness

The fracture toughness (K_{Ic}), which determines the resistance of the material to crack formation, is one of the material properties which requires special attention especially for applications such as medical implants using metal-on-metal articulation. The indentation-fracture technique is a well-established and reliable method for characterization of this material property where the surface of the specimen is indented by a Vickers diamond and the impression is analyzed for crack propagation using scanning electron microscopy (SEM).

The fracture toughness values of all specimens are then calculated using the formula proposed in Ref. 24,

$$K_{Ic} = \delta\left(\frac{E}{H}\right)^{0.5}\left(\frac{P}{c^{3/2}}\right), \tag{3}$$

where E (N mm^{-2}) is the elastic modulus of the nitrided layer, H (N mm^{-2}) is the Vickers microhardness, P (N) is the fixed applied load, and c (mm) is the average radial crack length obtained from the indentation impression using SEM.

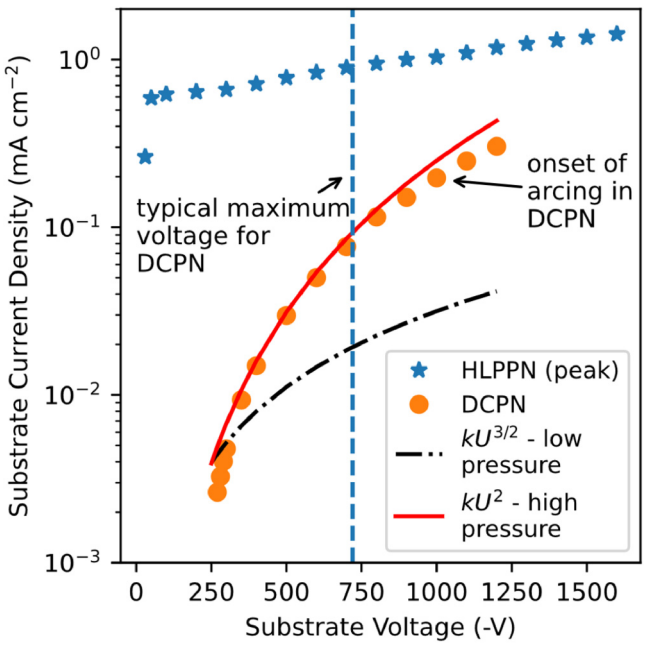

FIG. 4. Substrate current density as a function of the substrate voltage in HLPPN and conventional plasma nitriding (DCPN) environments. The solid line represents the current density calculated for DCPN where the pressure is high and collisions occur frequently in the sheath. The dotted-dashed line is the current density calculated at low pressure when there are no collisions in the sheath.

III. RESULTS AND DISCUSSION

A. Substrate current

In the two plasma nitriding regimes considered in this work, the substrate assumes different roles. In the conventional DCPN nitriding discharge, the substrate is the cathode that produces the plasma. In contrast, in the low-pressure plasma nitriding regime (HLPPN), its main role is to accelerate ions from a bulk plasma toward the substrate surface; the bulk plasma being produced by HIPIMS discharge. The substrate current comprises the flux of nitriding species, which determines the speed of nitriding, and its magnitude provides a direct quantitative comparison between the two plasma nitriding regimes.

Figure 3 illustrates the waveforms of the cathode voltage, cathode current, and substrate current during HLPPN. The substrate current peaks with a delay of ~20 μs with respect to the cathode current peak due to the time of flight required for ions to traverse the distance from the target to substrate.

The peak substrate current density in HLPPN, Fig. 4, is weakly affected by the substrate voltage. As the HIPIMS source is kept at constant operation parameters, it contributes constant flux. At low substrate bias $|U_B| < 400$ V, the substrate current is independent of substrate voltage. As the substrate voltage is increased beyond −400 V, an auxiliary plasma is ignited on the substrate surface, which produces additional flux, which by −1600 V reaches almost double the value at low bias. Comparing the increase and offset, it is clear that the majority of the plasma flux is provided by the HIPIMS source. The relatively constant ion flux at low bias voltages provides an opportunity to nitride parts at low voltages, particularly relevant for surfaces containing sharp features.

The constant current at low voltages can be attributed to the flat geometry of the substrate, which produces a correspondingly flat sheath. Ignoring edge effects, the area of the sheath is identical to the area of the substrate. Despite the increase in voltage, which is associated with an increase in sheath thickness, the collection area remains the same and the current to the substrate is proportional to the plasma density.

The Child–Langmuir law gives the ion current across a sheath and a high negative bias as $J_S \sim U_B^{3/2}$. This expression is valid at low pressure where ions traverse the sheath region without collisions and enter the sheath edge with a Bohm velocity acquired during flight through the presheath. Their energy is conserved

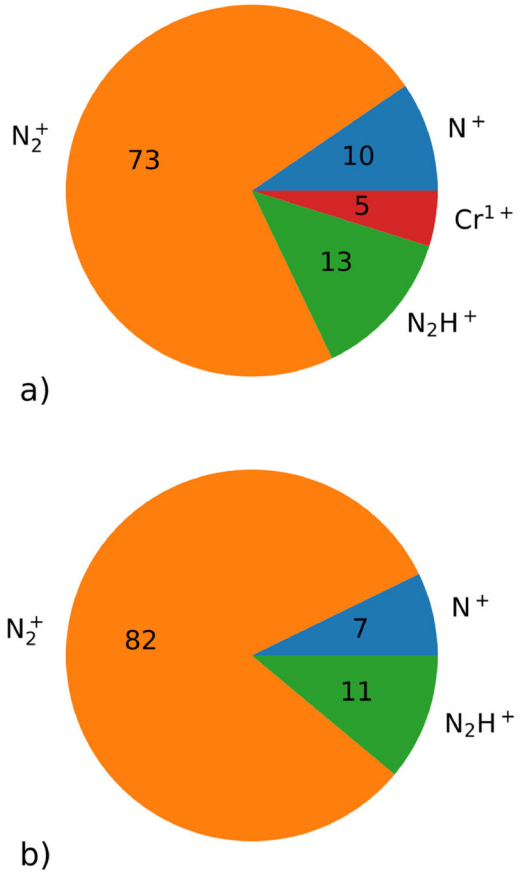

FIG. 5. Composition of the ion flux to the substrate in (a) HLPPN and (b) DCPN.

throughout the sheath. As shown in Fig. 4, the current above 400 V can be approximated by

$$J_S = \left(J_H + kU_B^{\frac{3}{2}}\right)(1 - \gamma_{SEE}), \tag{4}$$

where J_H is the ion saturation current collected from the HIPIMS-excited plasma, k is a constant of proportionality, and γ_{SEE} is the secondary electron emission coefficient. The second term is approximated by the Child–Langmuir law for low-pressure (collisionless) sheath. The secondary electron emission coefficient peaks at ~400 V and reduces slowly above those values.

During DCPN, the substrate current increases steeply with substrate voltage. A good fit to the data is achieved through the relation

$$J_S = kU_B^2. \tag{5}$$

At the high pressures commonly used in conventional plasma nitriding, the frequency of collisions is high, and ions undergo several collisions, whereby their energy is not conserved. Their flux into the sheath region is also reduced with velocity approaching thermal velocity and significantly lower than the Bohm velocity. At high pressure, the current and voltage in the sheath can be evaluated according to the following two assumptions.[25] The first one is that the ion mobility is independent of velocity and the pressure is so high that it is dominated by collisions with particles. The second is that there is no ionization in the sheath as the density of electrons is negligible on account of the highly negative potential in the sheath and high mobility of the electrons. The current continuity between the sheath edge and the substrate still holds, as expressed by

$$n_i u_i = n_s u_s, \tag{6}$$

where n_s is the ion density and u_s the velocity at the sheath edge, and n_i and u_i are the same quantities in the sheath. In a highly collisional case,

$$u_i = \mu_i E, \tag{7}$$

where μ_i is the ion mobility and E is the electric field. At the velocities and pressures of plasma nitriding, the mobility is relatively independent of velocity. Solving for u_i and substituting in Eq. (6), the ion density is

$$n_i = \frac{n_s u_s}{\mu_i E}. \tag{8}$$

Substituting in Gauss's law in one dimension, we obtain

$$\frac{dE}{dx} = \frac{e n_s u_s}{\varepsilon_0 \mu_i E}, \tag{9}$$

where x is the distance across the sheath, e is the electron charge, and ε_0 is the permittivity of free space. By integrating and solving for E, we obtain

$$E = \left(\frac{2 e n_s u_s}{\varepsilon_0 \mu_i}\right)^{1/2} x^{1/2}, \tag{10}$$

where $E(0) = 0$ at the sheath edge. We can evaluate the potential, Φ, through a second integration

$$\Phi = \left(\frac{2 e n_s u_s}{\varepsilon_0 \mu_i}\right)^{1/2} \frac{2}{3} s^{3/2}, \tag{11}$$

where we have assumed $\Phi(0) = 0$ at the sheath edge and $x = s$ at the electrode position. Recognizing that the ion current at the sheath edge is $J_S = e n_s u_s$ and the voltage at the electrode position is $U_s = -\Phi$, we have

$$J_S = \frac{9}{8} \varepsilon_0 \mu_i \frac{U_B^2}{s^3}. \tag{12}$$

This fits well with the experimentally obtained fit in Eq. (5). A strong variation in current with voltage means that ion flux and energy cannot be controlled independently.

It is worth noting that the experiments were restricted to voltages under 1000 V as beyond that, the probability of glow-to-arc transition increased substantially resulting in frequent arcing on the substrate surface and suggesting a limit where the technology can be applied. Furthermore, state-of-the-art systems in the field confine themselves to <700 V. At this substrate bias, HLPPN produces a substrate ion flux that is a factor of 17 greater than conventional plasma nitriding, indicating significantly faster nitriding rates would be expected.

B. Plasma composition

Near the substrate, the main ion constituents of the plasma were N_2^+, N_2H^+, and N^+ as shown in Fig. 5. The relative flux of dissociated nitrogen was significant for HLPPN with ratios of N^+:$N_2^+ = 0.12$ and N^+:$N_2H^+ = 0.75$, representing an enhancement by 150% and 120%, respectively, compared to DCPN.

C. Plasma density and electron temperature in HLPPN

The density and electron temperature of the bulk plasma between the magnetron cathode and the substrate were evaluated for different levels of substrate bias and constant magnetron discharge parameters. Figure 6 shows that at the peak of the HLPPN current pulse, the plasma density was in the range $1.1–1.3 \times 10^{12}$ cm^{-3} and was not strongly correlated with the substrate bias voltage.

The electron temperature in HLPPN was in the range of 6 ± 0.5 eV and exhibited very little dependence on the bias voltage within the investigated range of −400 and −1200 V.

The temporal evolution studies of plasma density during the HLPPN pulse (not shown) confirm the independence of plasma density from the substrate bias voltages in the range of −600 and −1200 V.

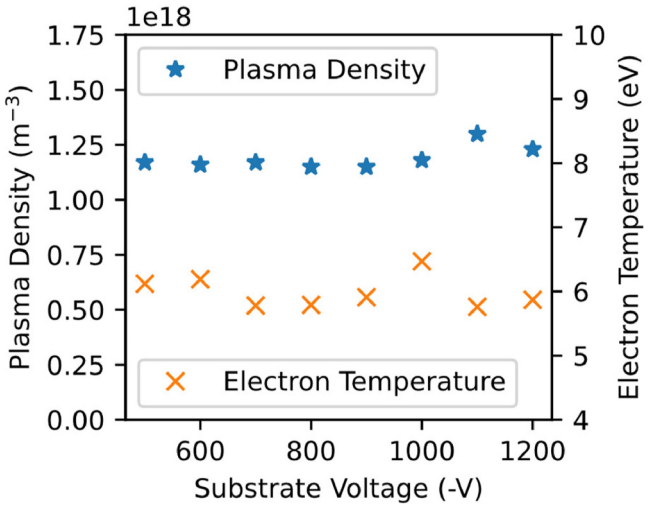

FIG. 6. Plasma density and electron temperature in HIPIMS-enhanced low-pressure plasma nitriding as a function of substrate voltage.

The observations of plasma density and electron temperature indicate that in HLPPN, the bulk plasma was relatively unperturbed by the presence of very high bias at the substrate. At these low pressures of 8.3×10^{-3} mbar, the substrate bias alone was unable to initiate a discharge without the auxiliary plasma of the magnetron. In line with the quasistationary nature of magnetron discharges, the plasma is created near the cathode surface and in the electromagnetic trap of the magnetron, independent of the substrate or chamber beyond the immediate vicinity of the cathode. The plasma chemistry and density are established according to the conditions at the target. The plasma then diffuses toward the substrate, and ions drifting into the substrate sheath are accelerated across the substrate potential to be implanted into the substrate.

D. Ion energy distribution function in HLPPN and DCPN

The ion energy distribution function (IEDF) for the main ions found in the plasma is compared in Fig. 7 for HLPPN (a) and DCPN (b). In both discharges, there is an appreciable ion flux at low energy.

However, it is remarkable that only the HLPPN case is found to produce high-energy ions with energy equivalent to the substrate bias voltage. For N_2H^+, N^+, and Cr^{1+}, the flux of high-energy ions is more intense than the low-energy ions [Fig. 7(a)]. For N_2^+, the magnitudes of the high-energy and low-energy ions are similar. In DCPN, the flux of high-energy ions is negligible for all species [Fig. 7(b)]. At high energy, the most abundant ions are N^+, which is highly active; however, it comprises 1% of the total flux for that species.

E. Discussion on plasma environment

The plasma investigations have revealed fundamental differences in the magnitude and energy of the ion flux produced by HIPIMS-enhanced low-pressure plasma nitriding and the conventional plasma nitriding processes, which can explain the accelerated nitriding rates observed in HLPPN. The magnitude of the ion flux is increased by a factor of 17 in HLPPN compared to DCPN at a control voltage of −700 V due to the efficient plasma generation source deployed in HLPPN based on magnetron cathode and the utilization of high-power density delivered in pulses. Plasma chemistry evaluation (Sec. III B) shows that the ion flux comprises highly active species such as N^+, N_2H^+, and N_2^+, which are particularly effective in nitriding.

The energy of the arriving ions is significantly enhanced in HLPPN compared to DCPN due to the substantial differences in operational pressure of the two techniques. HLPPN is capable of operating at lower pressure of 8.3×10^{-3} mbar due to the high efficiency of the magnetron plasma source and high-density of the plasma it produces (Sec. III C). The plasma source also provides a means of independently selecting the magnitude and energy of the nitriding flux. Operating at low pressure means that there is a long mean free path of molecular elastic scattering, which exceeds the size of the sheath, thereby allowing ions to accelerate to the full potential available across the sheath. This observation is supported by both the substrate current and ion energy distribution function measurements in Secs. III A and III D, respectively, as follows.

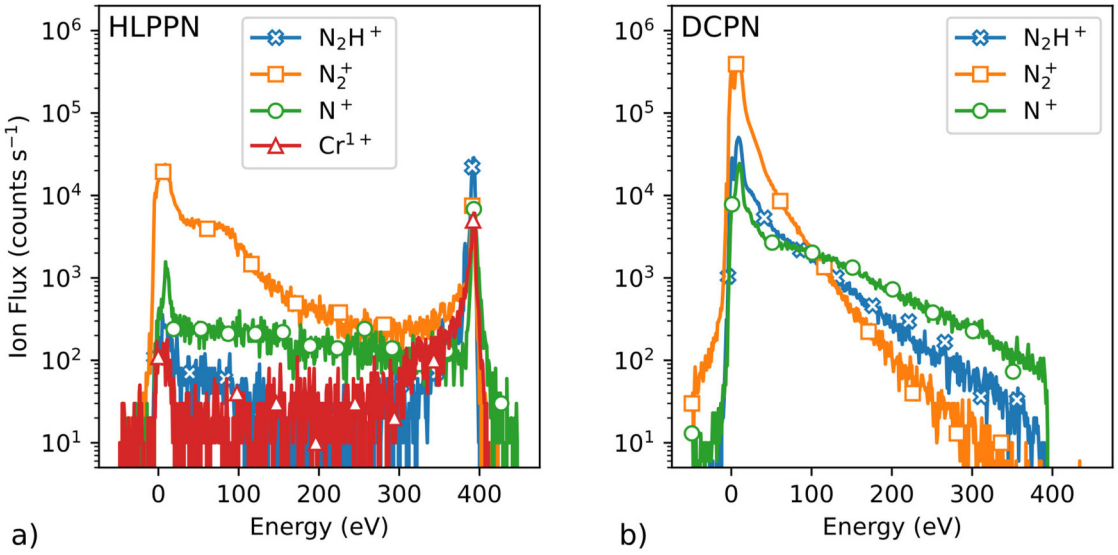

FIG. 7. Ion energy distribution function at the substrate surface biased to −400 V in (a) HLPPN and (b) DCPN.

Section III A showed that the substrate current and voltage were related as $J_S = \left(J_H + kU_B^{\frac{3}{2}}\right)$, with the exponent 3/2 being indicative of a collisionless sheath. This is confirmed by the IEDF analysis in Sec. III D, which showed that the majority of the ions were accelerating to the full bias potential applied to the surface. At typical nitriding voltages of −1000 V, these ions gain sufficient energy to be implanted into the surface prior to diffusing into the bulk, thus enhancing the retention rate of ions and promoting a higher concentration in the substrate alloy. In addition, the analysis of the chemistry of the flux showed that these highly energetic ions are also active radicals such as N^+, and N_2H^+, which have high diffusion rates into the substrate alloy. The high-energy ion bombardment also creates surface and bulk vacancies,[26,27] which accelerate diffusion and enhance both the case depth and maximum nitrogen concentration. At the same time, the relatively low mass of the ions means that the resputtering rate of the substrate is low, thus losses of nitrided material are low.

In contrast, the DCPN case appears to be completely bereft of high energy ions. Here, igniting and sustaining the discharge require an operating pressure of 9.3×10^{-2} mbar, which is one order of magnitude higher compared to HLPPN because there is no means of enhancing ionization such as a plasma source or magnetic confinement fields. The high operating pressure in DCPN dictates that within the sheath, there are frequent molecular collisions that interrupt the acceleration of ions by the electrical field in the sheath, and practically, no ions are able to gain the full energy of the bias voltage. Active species arrive at the substrate at very low energy and diffusion rates are slow due to the absence of accelerating factors such as ion implantation and vacancy-induced diffusion. Some industrial DCPN in the field are carried out at a pressure of 2–5 mbar as standard—a factor of 20–50 higher than the measurements reported here. In these cases, we expect the loss of ion energy due to collisions in the sheath to be even more pronounced.

F. Properties of the plasma nitrided layer produced by utilizing HIPIMS discharge

As already articulated in the introduction of this article, the advantages of the nitriding treatment are the enhanced hardness and corrosion resistance of the nitrided case when compared to the properties of the core material. It was shown that nitriding can be used as a single treatment but often is combined with coating in a duplex treatment process where the load-bearing capacity of the substrate is largely improved, leading to overall component lifetime and performance improvement. The ever-growing demand for medical implants based on metal-on-metal articulation motivated the authors to apply the new technology for plasma nitriding based on the utilization of HIPIMS discharge to treat medical-grade CoCrMo alloy. The detailed results of this research have already been published elsewhere.[28–31] The following provides a brief summary of the properties and the performance of such plasma treated surfaces.

G. Phase composition of the nitrided layer

XRD data of the untreated CoCrMo substrate (not included here) showed a predominantly face-centered cubic (fcc) structure, called γ austenite phase along with a hexagonal closed-packed (HCP) structure, called the ϵ phase, which is typical for this alloy as reported elsewhere.[32]

The phase composition of the treated alloy depends on the bias voltage applied during the nitriding process. The results from thorough analyses in a wide range of bias voltages from Ub = –500

to −1100 V have been previously reported in detail by the authors elsewhere.[29] The best mechanical, tribological, and barrier properties were achieved for nitriding in the bias voltage range (from −700 to −1100 V), where γ_N (111) and γ_N (200) peaks were identified corresponding to the expanded austenite phase.

The texture analyses revealed that at a lower bias voltage of −700 V, the predominant crystallographic orientation of the nitrided layer is (200), whereas at higher bias voltages (from −900 to −1100 V), the layer developed mixed (111) and (200) texture.

H. Layer thickness and constitution

Cross-sectional SEM analysis was used to image the nitrided case depth produced in the CoCrMo alloy by HLPPN and DCPN. In both images, the plasma nitrided layer containing a mixture of $Co_4N + Co_{2-3}N$ is clearly visible as a top layer over the CoCrMo substrate. In the HLPPN, a thin bright-contrast diffusion layer of Co_4N is also present at the substrate/nitrided case interface. The analyses demonstrated that conventional plasma nitriding (DCPN) produced a nitrided case depth of 2.1 μm in 18 h, as shown in Fig. 8, whereas the HLPPN process produced a case depth of 2.5 μm in 4 h, which represents more than a factor of four increase in process productivity. This staggering process productivity increase can be attributed to the highly enhanced plasma reactivity, high ion flux, and high ion energy revealed by the plasma analyses of the HLPPN process discussed in Sec. III E. It has been shown that there is a factor 10 increase in ion flux, the presence of ions with energy of several hundred volts and a significant increase of the relative flux of dissociated nitrogen for HLPPN with ratios of N^+: $N_2 = 0.12$ enhanced by 150% compared to DCPN.

In addition to the enhanced layer growth rate, the nitrogen concentration in the nitrided layer at a control depth of 1.5 μm was found to be a factor of 2 higher for HLPPN than DCPN, as confirmed by SIMS chemical depth profile analyses (Fig. 9).[28] The relatively high concentrations of nitrogen embedded in the modified layer enable the use of process parameters, such as the accelerating bias voltage applied to the substrates, as a means to tailor the phase composition, extending from a pure S phase (Co_4N or γ_N phase) to a compound layer ($Co_4N + Co_{2-3}N$) as revealed by XRD analyses.[32]

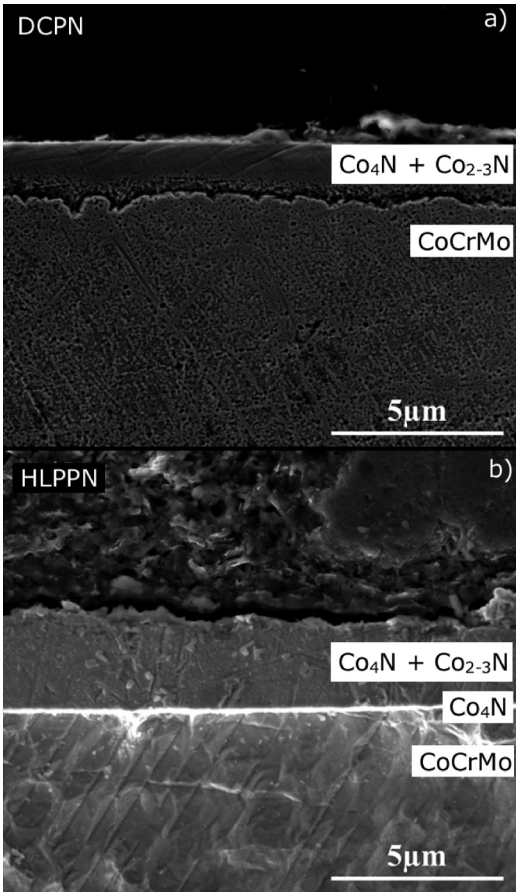

FIG. 8. Cross section SEM showing the thickness of the nitrided case produced by (a) conventional plasma nitriding (DCPN) and (b) HIPIMS-enhanced plasma nitriding, HLPPN techniques.

I. Layer mechanical properties

1. Layer hardness

Nanoindentation hardness measurements revealed that the HLPPN treatment resulted in higher instrumental hardness of $H_{IT} = 23$ GPa as compared to 20 GPa achieved for DCPN, which is substantially higher than that measured for the untreated alloy (7.9 GPa).

2. Nitrided layer tribological properties

The experiments revealed that the HLPPN treatment resulted in a noticeable improvement in dry sliding wear coefficient

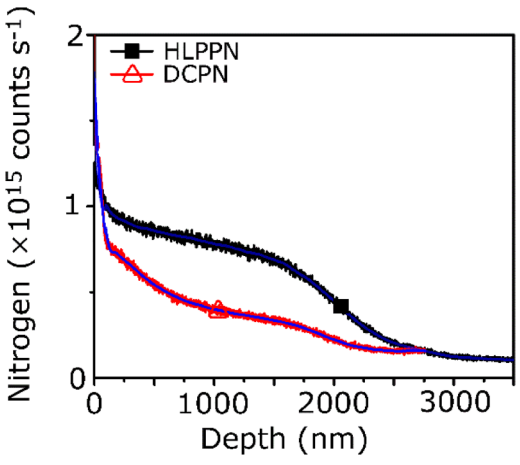

FIG. 9. SIMS compositional depth profile of DCPN and HLPPN. Compared to DCPN, HLPPN produces almost a factor of 2 higher nitrogen concentration in the nitrided layer at the control depth of 1.5 μm (Ref. 28). Reused with permission from Hovsepian *et al.*, Mater. Lett. **313**, 131782 (2022). Copyright 2022 Elsevier.

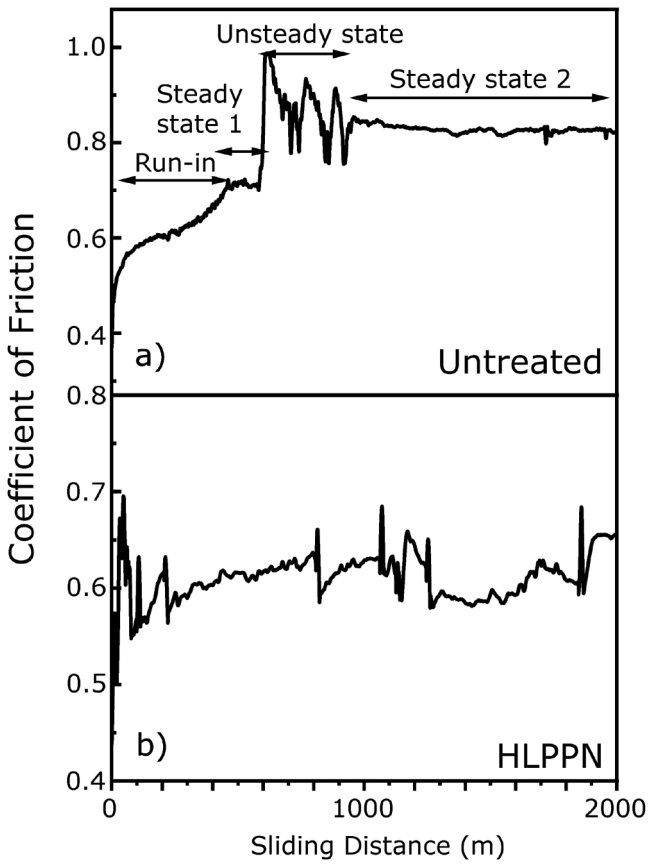

FIG. 10. Coefficient of friction *vs* sliding distance in dry sliding: (a) untreated and (b) HLPPN-treated CoCrMo alloy (Ref. 28). Reused with permission from Hovsepian *et al.*, Mater. Lett. **313**, 131782 (2022). Copyright 2022 Elsevier.

of ($K_C = 1.18 \times 10^{-15}$ m^3 N^{-1} m^{-1}) as compared to DCPN ($K_C = 2.2 \times 10^{-15}$ m^3 N^{-1} m^{-1}), whereas the improvement over the untreated specimens reached almost one order of magnitude higher ($K_{C\ \text{untreated CoCrMo alloy}} = 6.0 \times 10^{-14}$ m^3 N^{-1} m^{-1}). Similar enhancement of the tribological performance resulting from the HLPPN treatment was evident in the coefficient of friction behavior in dry sliding test conditions. As demonstrated in Fig. 10, the friction curve of the untreated alloy showed a very quick (sliding distance of only 600 m) transition from the run-in state to very high coefficient of friction values ($\mu = 1.0$) typically associated with the catastrophic failure of the material under test. In the following steady-state regime, the coefficient of friction remained high at $\mu = 0.82$. In contrast, the friction curve of the HLPPN-treated alloy was less erratic showing a stable low coefficient of friction value of $\mu = 0.6$ over the entire sliding distance of 2 km. The DCPN-treated samples exhibited a similar coefficient of friction[28] of $\mu = 0.6$. This study clearly demonstrates the higher quality of the HLPPN-produced nitrided layer and, therefore, the advantages of the novel technology.

3. Layer fracture toughness

The fracture toughness (K_{Ic}), which determines the resistance of the material to crack formation, is one of the material properties that requires special attention especially for applications such as medical implants using metal-on-metal articulation. The indentation-fracture technique is a well-established and reliable method for the characterization of this material property where the surface of the specimen is indented by a Vickers diamond and the impression is analyzed for crack propagation using SEM.

The SEM images in Fig. 11 illustrate the pattern of crack formation around the corners and edges of impressions from Vickers diamond indentations produced under a high normal load of 500 N on the surface of the untreated CoCrMo alloy and the nitrided layers produced by the HLPPN and DCPN techniques.

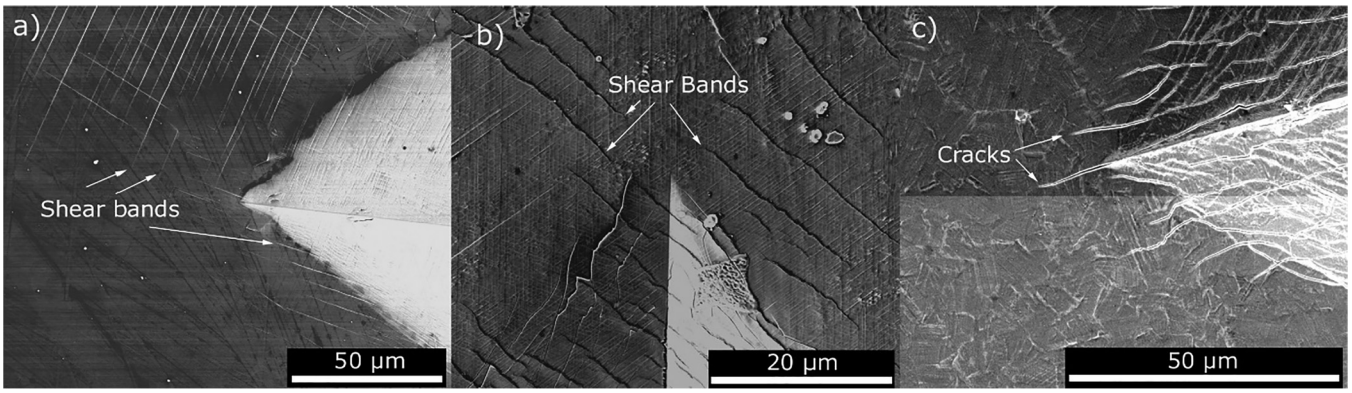

FIG. 11. SEM images of Vickers diamond indenter impressions (500 N load): (a) untreated CoCrMo alloy, (b) HLPPN treated, and (c) DCPN treated (Ref. 28). Reused with permission from Hovsepian *et al.*, Mater. Lett. **313**, 131782 (2022). Copyright 2022 Elsevier.

The application of an abnormally high normal load of 500 N to indent the surface, in this case, substantially improves the measurement accuracy. On the surface of the untreated alloy, only shear bands formed due to the plastic flow of the indented material, but no cracks were developed around the corners of the impression, which is attributed to the ductile nature of the CoCrMo alloy, Fig. 11(a). Figure 11(b) shows that the area around the corner of the impression for the HLPPN layer, despite the plastic deformation evidenced by the presence of shear bands, is also crack-free, demonstrating the higher layer toughness. In contrast, the DCPN layer exhibits a high crack density, which is typical of brittle materials [Fig. 11(c)].

In the conditions of the experiment, the untreated alloy showed a K_{Ic} value of around 908 MPa mm$^{1/2}$, which was relatively high considering the hardness of the alloy in the untreated state. Under the same conditions, the highest K_{Ic} value of 955 MPa mm$^{1/2}$ was obtained for the HIPIMS nitrided (HLPPN) alloy. The commercially nitrided specimen (DCPN) showed around 5% lower value than that of HLPPN. The relatively high values of the ratios between the hardness and elastic modulus H/E and H^3/E^2 of 0.078 and 0.135, respectively, which have been obtained for the nitrided layers produced by HLPPN, further confirmed the results from the calculation of the K_{Ic} values that the treatment enhances the toughness of the material.[33,34]

4. Layer barrier properties, corrosion resistance, and metal ion release

The electrochemical potentiodynamic polarization curves recorded for the various nitrided samples and the bare CoCrMo alloy are shown in Fig. 12. In the conditions of this experiment, the HLPPN-treated alloy showed a significant improvement in corrosion resistance with corrosion potential of $E_{Corr} = -218$ mV, which is considerably nobler compared to the untreated alloy ($E_{Corr} = -775$ mV) and similar to DCPN, and a higher pitting potential, Ep = 770 compared to 200 mV for the untreated alloy and even higher for DCPN. Similarly, the corrosion current densities measured for the HLPPN nitrided alloy of ($I_{Corr} = 5 \times 10^{-5}$ mA cm^{-2}) were found to be 2 orders of magnitude lower than the untreated CoCrMo alloy ($I_{Corr} = 2 \times 10^{-3}$ mA cm^{-2}) and factor 2 lower than DCPN nitrided alloy ($I_{Corr} = 1 \times 10^{-4}$ mA cm^{-2}). The results as expected also clearly demonstrated that the nitriding itself, irrespective of the technology, had a beneficial effect on the corrosion resistance of the alloy.

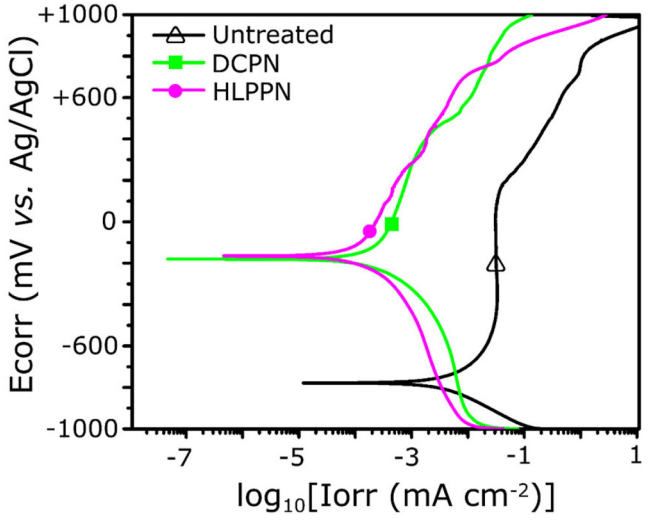

FIG. 12. Potentiodynamic polarization curves obtained in Hank's solution (*p*H:7.3) for CoCrMo alloy samples: untreated and after treatment by DCPN and HLPPN.

The effectiveness of the plasma nitriding treatment as a barrier against the metal ion release from the CoCrMo alloy in the biological environment was evaluated using ICP-MS analysis to determine the concentrations of metal ions in the electrolyte (Hank's solution) used in the potentiodynamic corrosion tests. The data showed that the rate of metal ion release from the HLPPN-treated samples was reduced by a factor of 2, 4, and 10 for Co, Cr, and Mo ions, respectively. The analyses clearly demonstrated that the new HLPPN treatment produces layers, which encapsulate effectively the CoCrMo substrate and act as a reliable barrier against metal ion release when immersed in a biological environment.

IV. SUMMARY AND CONCLUSIONS

- Using extensive plasma diagnostics, this work demonstrates for the first time that a HIPIMS discharge can be successfully utilized not only as a coating deposition technique but also as a plasma enhanced thermochemical treatment for surface material property modification.
- Plasma characterization revealed that at the control bias voltage of Ub = − 700 V, HLPPN produces a substrate ion flux that is a factor of 17 greater than conventional plasma nitriding (DCPN).
- However, the plasma composition of the HLPPN and DCPN is similar the total energy delivered on the surface by the reactive ions in DCPN is several orders of magnitude lower as compared to the HLPPN case.
- The relative flux of dissociated nitrogen was significant for HLPPN with ratios of $N^+:N_2^+ = 0.12$ and $N^+:N_2H^+ = 0.75$.
- In HLPPN, the energy of nitriding species arriving at the surface is equivalent to the bias voltage on the substrate and sufficient to promote implantation, whereas in DCPN, it is severely diminished and confined to a few electron volts.
- The nitriding rate of the HLPPN process was found to be a factor of 4 higher than that of the industry-standard DCPN treatment used as a benchmark.
- Compared to DCPN, HLPPN achieves almost a factor of 2 higher nitrogen concentration in the nitrided layer at a control depth of 1.5 μm.
- HLPPN-produced nitrided layers show higher hardness (H_{IT} = 23 GPa) and higher wear resistance (lower wear coefficient $Kc = 1.18 \times 10^{-15}$ m^3 N^{-1} m^{-1}) as compared to the DCPN process ($Kc = 2.2 \times 10^{-15}$ m^3 N^{-1} m^{-1}).
- The obtained high H/E and H^3/E^2 values of 0.078 and 0.135, respectively, are indicative of a high fracture toughness of the nitrided layers produced by the utilization of the novel HLPPN technology.

- With higher corrosion potential, ECorr = 160 mV, and higher pitting potential, Ep = 770 mV, the HLPPN layers showed a superior corrosion performance in Hank's solution, providing reliable corrosion protection of the untreated CoCrMo alloy.
- The enhanced mechanical and corrosion resistance properties and favorable Me-ion release performance combined with the significant enhancement in process productivity make the HIPIMS-enhanced plasma nitriding a powerful technique for surface treatment of medical-grade CoCrMo alloys.
- Finally, the novel HIPIMS enhanced plasma nitriding process is ideal for developing duplex surface treatment technologies integrating surface nitriding and functional coating deposition in a single unit.

ACKNOWLEDGMENTS

The authors would like to acknowledge Zimmer-Biomet, UK for providing financial support as well as for the highly inspirational and fruitful discussions in the course of this research. The authors gratefully acknowledge the valuable advice of Claire Greenwood, Product Manager in the Plasma & Surface Analysis Division at Hiden Analytical Ltd (UK), for obtaining ion energy distributions at an electrically biased surface. For the purpose of open access, the author has applied a Creative Commons Attribution (CC BY) license to any Author Accepted Manuscript version arising from this submission.

AUTHOR DECLARATIONS

Conflicts of Interest

The authors have no conflicts to disclose.

Author Contributions

A. P. Ehiasarian: Conceptualization (equal); Data curation (equal); Investigation (equal); Methodology (equal); Writing – original draft (equal); Writing – review & editing (equal). **P. Eh. Hovsepian:** Conceptualization (lead); Data curation (equal); Formal analysis (equal); Investigation (equal); Methodology (equal); Supervision (equal); Writing – original draft (equal); Writing – review & editing (equal).

DATA AVAILABILITY

The data that support the findings of this study are available from the corresponding author upon reasonable request.

REFERENCES

[1]B. Berghaus, German Patent No. DPR 668,639 (20 July 1932).
[2]B. Chapman, *Glow Discharge Processes* (Wiley, New York, 1980).
[3]L. Zagonel, C. Figueroa, R. Droppajr, and F. Alvarez, Surf. Coat. Technol. **201**, 452 (2006).
[4]E. Menthe, A. Bulak, J. Olfe, A. Zimmermann, and K. T. Rie, Surf. Coat. Technol. **133**, 259 (2000).
[5]A. Grill and D. Itzhak, Thin Solid Films **101**, 219 (1983).
[6]A. Leyland, K. S. Fancey, A. S. James, and A. Matthews, Surf. Coat. Technol. **41**, 295 (1990).
[7]M. K. Lei and Z. L. Zhang, J. Vac. Sci. Technol. A **13**, 2986 (1995).
[8]K. O. Legg, H. Solincs-Legg, T. S. Sudarshan, and G.H. Bhat, "Trends in ion implantation and ion-assisted coatings," in *Proceedings of the 1st International Conference on Surface Modification Technologies*, Phoenix, AZ, January 1988 (The Metallurgical Society of AIME, Warrendale, PA, 1988).
[9]H. R. Kaufman, J. Vac. Sci. Technol. **15**, 272 (1978).
[10]J. R. Conrad, S. Baumann, R. Fleming, and G. P. Meeker, J. Appl. Phys. **65**, 1707 (1989).
[11]E. Moll and H. Daxinger, U.S. patent 4,197,175 (1977).
[12]N. Renevier, P. Colligon, H. Michel, and T. Czerwiec, Surf. Coat. Technol. **111**, 128 (1999).
[13]J. D. Kamminga, D. Doerwald, M. Schreurs, and G. C. A. M. Janssen, Surf. Coat. Technol. **200**, 1837 (2005).
[14]R. Wei, T. Booker, C. Rincon, and J. Arps, Surf. Coat. Technol. **186**, 305 (2004).
[15]J.-D. Kamminga, R. Hoy, R. G, C. A. M. Janssen, E. Lugscheider, and M. Maes, Surf. Coat. Technol. **174–175**, 671 (2003).
[16]A. P. Ehiasarian, "Plasma surface engineering research and its practical applications," in *Fundamentals and Applications of High-Power Impulse Magnetron Sputtering*, edited by R. Wei (Research Signpost, Trivandrum, 2007).
[17]A. P. Ehiasarian and R. Bugyi, "Industrial size high power impulse magnetron sputtering," in *Proceedings of the 47th Annual Technical Conference of the Society of Vacuum Coaters*, Dallas, TX, 24–29 April 2004 (Society of Vacuum Coaters, Dallas, TX, 2004), p. 437.
[18]A. P. Ehiasarian and P. Eh. Hovsepian, "Plasma nitriding by HIPIMS discharge," Sheffield Hallam University Technical Report, Sheffield, UK, 2005.
[19]A. P. Ehiasarian, R. Tietema, R. Bugyi, A. Klimczak, P. Eh. Hovsepian, and D. Doerwald, China Patent No. ZL2007,80,012,990.9 (10 April 2007).
[20]A. P. Ehiasarian, J. G. Wen, and I. Petrov, J. Appl. Phys. **101**, 054301 (2007).
[21]P. Eh. Hovsepian, A. A. Sugumaran, Y. Purandare, D. A. L. Loch, and A. P. Ehiasarian, Thin Solid Films **562**, 132 (2014).
[22]D. B. Lewis, L. A. Donohue, M. I. Lembke, W-D Münz, R. Kužel, V. Valvoda, and C. J. Blomfield, Surf. Coat. Technol. **114**, 187 (1999).
[23]W. C. Oliver and G. M. Pharr, J. Mater. Res. **7**, 1564 (1992).
[24]S. Zhang, D. Sun, Y. Fu, and H. Du, Surf. Coat. Technol. **198**, 74 (2005).
[25]M. A. Lieberman and A. J. Lichtenberg, *Principles of Plasma Discharges and Materials Processing* (Wiley-Interscience, Hoboken, NJ, 2005).
[26]O. Rodríguez de la Fuente, M. A. González, and J. M. Rojo, Phys. Rev. B **63**, 085420 (2001).
[27]G. Abrasonis, J. P. Rivière, C. Templier, L. Pranevičius, and N. P. Barradas, J. Appl. Phys. **97**, 124906 (2005).
[28]P. Eh. Hovsepian, K. Shukla, A. Sugumaran, Y. Purandare, I. Khan, and A. P. Ehiasarian, Mater. Lett. **313**, 131782 (2022).
[29]K. Shukla, A. Sugumaran, I. Khan, A. Ehiasarian, and P. Hovsepian, J. Mech. Behav. Biomed. **111**, 104004 (2020).
[30]A. Sugumaran, K. Shukla, I. Khan, A. Ehiasarian, and P. Hovsepian, Vacuum **185**, 109994 (2020).
[31]K. Shukla, Y. Purandare, I. Khan, A. Ehiasarian, and P. Hovsepian, Surf. Coat. Technol. **400**, 126227 (2020).
[32]M. Jenko, M. Gorensek, M. Godec, M. Hodnik, B. Setina Batic, C. Donik, J. T. Grant, and D. Dolinar, Appl. Surf. Sci. **427**, 584 (2018).
[33]X. Chen, Y. Du, and Y. W. Chung, Thin Solid Films **688**, 137265 (2019).
[34]A. Leyland and A. Matthews, Wear **246**, 1 (2000).